Sensor redundancy based FDI using an LPV sliding mode observer

L. Chen* and C. Edwards and H. Alwi

College of Engineering, Mathematics and Physical Sciences, University of Exeter, UK

SUMMARY

In this paper, a linear parameter varying (LPV) sliding mode sensor fault detection and isolation (FDI) scheme is proposed wherein knowledge of the measurement redundancy is utilised to achieve FDI in multiple channels simultaneously. Such a situation is common in some state-of-the-art aircraft fault diagnosis systems where information is generally/mainly measured based on triplex redundancy. The scheme proposed in this paper is based on an LPV sliding mode observer and exploits the so-called equivalent output error injection signal to create estimates of the measurement faults. In the case of sensor measurement redundancy, and where there exists a fault free (but unknown) sensor amongst the set of measurements, the fault reconstruction performance of the observer can be improved by isolating and using the output error injection signal associated with the fault free redundant sensor. Simulation results using the RECONFIGURE benchmark model demonstrate the effectiveness of the scheme.

KEY WORDS: Integral sliding mode; Fault tolerant control; Control allocation

1. MOTIVATION

In recent years, LPV sliding mode observers have been developed to detect and isolate actuator or sensor faults/failures over a large range of plant operation conditions [1, 2]. These observers contain nonlinear injection terms driven by the output estimation errors and are quite different from the Luenberger LPV observers which exist in the literature (e.g. [3, 4, 5, 6, 7, 8, 9, 10, 11, 12, 13]). Sliding mode observers typically create a residual signal which is robust against uncertainties so that faults/failures can be reconstructed rather than just being detected. Furthermore the system states can be robustly estimated despite the existence of faults if they can be expressed as matched uncertainties with respect to the measurements. Usually, the thresholds used to declare faults are chosen adaptively to satisfy the requirements of early detection, low missed detection rates and false alarm rates, to further enhance the detection performance (e.g. in [14]). These advantages have been demonstrated during the EU-FP7 ADDSAFE project [15]. *However, one of the lessons learnt from the ADDSAFE project relating to sensor FDI, is that because of the uncertainty, the isolation logic required to determine the source of the faults from the three available sensors is challenging and computationally intensive and contributes to more of the execution time than the*

*Correspondence to: College of Engineering, Mathematics and Physical Sciences, University of Exeter, UK.

underlying observer design itself. This results in the schemes being considered as 'expensive' in terms of computation time in the flight control computer [16].

In this paper, an LPV sliding mode observer based scheme is developed based on directly exploiting *sensor redundancy in the context of direct duplication making the scheme much simpler and with lower computation complexity as compared to [15].* In ADDSAFE a sensor benchmark problem was developed based on a triplex redundancy configuration and voting logic (as shown in Fig. 1). Such measurement devices are commonly used in state-of-the-art fault diagnosis systems. In this paper the observer scheme allows multiple simultaneous sensor measurement faults within the triplex system to be detected and isolated. Compared with [15], the scheme proposed in this paper does not require significant extra logic blocks to isolate the location of the faults because *a single observer* is driven by all three (redundant and potentially faulty) sensor signals rather than a single voted signal. Furthermore, the scheme proposed here has the capability of reconstructing faults in multiple channels simultaneously, which cannot be done using the scheme in [15]. Despite the fact that the observer proposed in this paper has a higher state-space order than the one in [15] due to the redundant sensor measurements that are used to drive the observer, the final scheme has a significantly lower computational load in terms of industrial implementation and therefore a faster execution time. This is because extensive post-processing of the reconstruction signals in [15] is no longer necessary. In contrast to [17], it is assumed the sensor providing the measurement for the LPV scheduling parameters are healthy and provide accurate values [15]. (Indeed this assumption is true in much of the LPV literature).

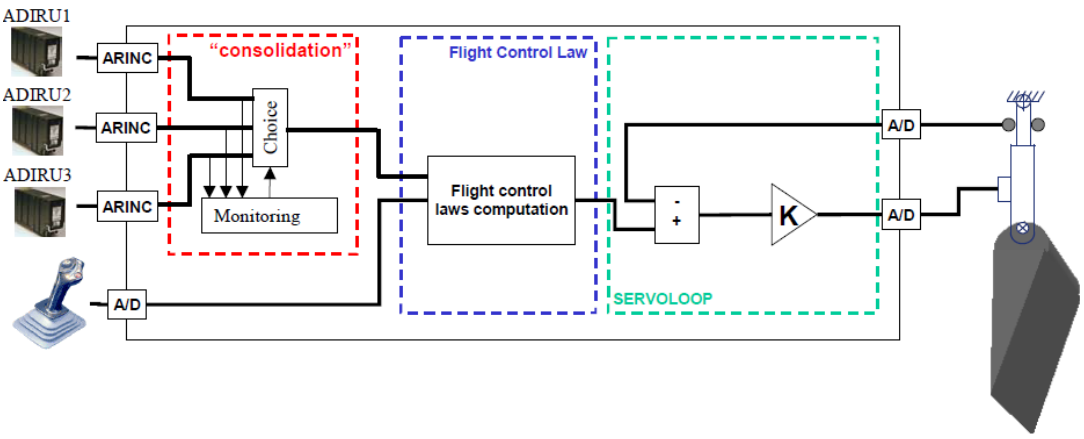

Figure 1. Airbus triplex redundancy configuration and the consolidation logic [18]

It is well known in the fault detection literature that if faults and uncertainties share the same channel, traditional observer designs (without using sensor redundancy) cannot distinguish between faults and uncertainties, and therefore 'clean' fault reconstruction signals are difficult to obtain. In this study, we propose the equivalent error injection signal associated with fault free sensors is utilised to reconstruct the uncertainty signal located in the fault free channel. The uncertainty reconstruction signal is then employed to 'cancel' uncertainties appearing in the faulty channels so that 'clean' fault reconstruction signals can be obtained. The problem set-up in this paper is non-standard because the measured outputs are not independent from a system theory perspective.

This requires some further initial theoretical development to rigorously understand this 'unusual' configuration, since at first glance, the theory in [1, 2] and hence [15] is not directly applicable.

This paper also attempts to bridge the gap between existing fault detection schemes and the aerospace industry demands for sensor FDI. In current Airbus industrial practice, triplex redundant air data sensor measurements are available and the fault detection logic (consolidation process) requires at least two data channels to be fault-free. In the case wherein two or more than two sensors fail simultaneously (and identically), the consolidation logic may become unreliable [19, 20, 21]. Instead of using the Airbus consolidation logic (in the work presented in [15], the sliding mode observer is driven by one consolidated sensor output), the consolidation logic can be replaced by the proposed scheme.

In this paper, a case study based on Airbus's RECONFIGURE benchmark is used to demonstrate the efficacy of the proposed scheme. In this study, two of the three angle of attack sensors are assumed to be simultaneously corrupted by various sensor faults. The simulation results show that not only can two faults be straightforwardly detected and isolated, but also the fault reconstruction performance can be improved for a large set of flight conditions. The contribution claimed here is not in terms of the development of the sliding mode observer per se, but its application within a novel problem formulation.

The paper is organised as follows: in Section 2 the new problem formulation is proposed for a generic LPV representation with redundant (identical) measurements; whilst Section 3 discusses the isolation logic associated with the proposed scheme. In Section 4, the decision making logic, used to improve the fault reconstruction performance in the presence of a fault free redundant sensor, is introduced. A case study based on the RECONFIGURE benchmark model is described in Section 5. Finally, Section 6 makes some concluding remarks and offers directions for future work.

2. LPV SLIDING MODE OBSERVER

Consider an LPV model of the plant represented by

$$\begin{aligned} \dot{x}_p(t) &= A_p(\rho)x_p(t) + B_p(\rho)u(t) + M_p(\rho)\zeta(t) \\ y_p(t) &= C_p x_p(t) + N_p f(t) \end{aligned} \tag{1}$$

where, $A_p(\rho) \in \mathbb{R}^{n\times n}$, $B_p(\rho) \in \mathbb{R}^{n\times m}$, $C_p \in \mathbb{R}^{p\times n}$ and $N_p \in \mathbb{R}^{p\times q}$, where $q < p$ and N_p represents the sensor fault distribution matrix. The time varying matrix $M_p(\rho) \in \mathbb{R}^{n\times d}$ represents the uncertainty distribution matrix. The vector $\rho \in \Theta \subset \mathbb{R}^h$ denotes the set of nominal scheduling parameters belonging to a polytope Θ. In (1) it is assumed that $y_p(t)$ and $u(t)$ are measurable but $x_p(t)$ is unknown. The signal $f(t)$ represents faults, which are unknown, and are to be estimated. The signal $\zeta(t)$ represents the uncertainty which is assumed to be bounded by $\|\zeta(t)\| \leq \beta$. The scheduling parameter ρ is assumed to be measured accurately (in contrast to [17]).

In this paper, all parameter varying matrices are assumed to depend affinely on ρ, in particular

$$A_p(\rho) = A_{p,0} + \rho_1 A_{p,1} + \ldots + \rho_h A_{p,h} \tag{2}$$

where, the scalar ρ_i represents the ith component of ρ.

Assumption 1
In the system in (1):

- the columns of N_p are taken from the standard basis for $\mathbb{R}^p$;
- $\mathrm{rank}(C_p) < p$, i.e. there exits redundancy within the measurements, and furthermore the matrix C_p has several identical rows corresponding to repeated identical sensors measuring the same quantity of interest.

Remark 1
As a consequence of Assumption 1, this paper is quite distinct from [1, 2] and [15] (and indeed all of the previous work of the authors) and requires some (preliminary) careful development to account for the rank deficiency in C_p. In the authors' earlier work, for example in [1, 2] and [15], *several different observers were designed and run in parallel* to account for the duplication of measurements. In this way the output distribution matrices in [1, 2] are of full (row) rank. The approach proposed here is quite different and the implicit rank deficiency is handled differently.

2.1. Observer structure with the rank deficiency in C_p

Because of the rank deficiency associated with C_p this subsection develops a bespoke framework because sliding cannot be sustained on the surface associated with the output estimation error being maintained at zero.

Exploiting the structure of N_p, and by permutating the system outputs, it is easy to obtain the output representation

$$\begin{bmatrix} y_{p,1}(t) \\ y_{p,2}(t) \end{bmatrix} = \begin{bmatrix} C_{p,1} \\ C_{p,2} \end{bmatrix} x_p(t) + \begin{bmatrix} 0 \\ I_q \end{bmatrix} f(t) \tag{3}$$

where $C_{p,1} \in \mathbb{R}^{(p-q)\times n}$ and $C_{p,2} \in \mathbb{R}^{q\times n}$, and $y_{p,2}(t)$ denotes the measurements potentially corrupted by sensor faults.

Assumption 2
It will be assumed that $y_{p,2}$ comprises multiple measurements of the same quantities by distinct identical sensors.

Remark 2
From Assumption 2, $C_{p,2}$ is rank 1 and formed from q identical rows. This will be exploited in all the analysis which follows. Such a situation occurs in many systems (such as aircraft) where critical information is measured by triplex redundant sensor systems [22], which here would correspond to $q = 3$. The ideas of [1, 2] and [15] cannot be directly applied to the formulation in (1)–(3). *This paper addresses and exploits this rank deficiency property in a bespoke way. A specific formulation is proposed to handle this situation, and this represents the main contribution of the paper.*

Suppose $\mathrm{rank}(C_{p,1}) = r \leq p - q$. As a consequence the matrix $C_{p,1}$ can be written as $C_{p,1} = QR$ where $Q \in \mathbb{R}^{(p-q)\times(p-q)}$ is a nonsingular square matrix and $R \in \mathbb{R}^{(p-q)\times n}$ has following structure

$$R = \begin{bmatrix} 0 \\ R_1 \end{bmatrix} \tag{4}$$

where $R_1 \in \mathbb{R}^{r\times n}$. Let $\tilde{y}_{p,1} = Q^{-1}y_{p,1}$, then $\tilde{y}_{p,1} = Rx_p$. Define a new state component $z_f(t) \in \mathbb{R}^q$ according to

$$\dot{z}_f(t) = -A_f z_f(t) + A_f y_{p,2}(t) \tag{5}$$

where $A_f = a_f I_q$ and a_f is a positive design scalar. From (1), (3) and (5), an augmented system can be created of the form

$$\begin{aligned}\begin{bmatrix}\dot{x}_p(t)\\ \dot{z}_f(t)\end{bmatrix} &= \begin{bmatrix}A_p(\rho) & 0\\ A_f C_{p,2} & -A_f\end{bmatrix}\begin{bmatrix}x_p(t)\\ z_f(t)\end{bmatrix} + \begin{bmatrix}B_p(\rho)\\ 0\end{bmatrix}u(t) + \begin{bmatrix}0\\ A_f\end{bmatrix}f(t) + \begin{bmatrix}M_p(\rho)\\ 0\end{bmatrix}\zeta(t)\\ \begin{bmatrix}\tilde{y}_{p,1}(t)\\ z_f(t)\end{bmatrix} &= \begin{bmatrix}R & 0\\ 0 & I_q\end{bmatrix}\begin{bmatrix}x_p(t)\\ z_f(t)\end{bmatrix}\end{aligned} \tag{6}$$

Define a coordinate transformation matrix for (6) by

$$T_a = \text{Diag}\{T_s, I_q\} \tag{7}$$

where $T_s \in \mathbb{R}^{n\times n}$ is any nonsingular matrix such that $R_1 T_s^{-1} = \begin{bmatrix} 0 & I_r \end{bmatrix}$. Let $A_f C_{p,2} T_s^{-1} = \begin{bmatrix} A_{31} & A_{32}\end{bmatrix}$. Because $A_f = a_f I_q$ where a_f is a scalar, the matrix sub-block A_{31} is formed from repeated rows; i.e. it has the from $\mathbf{1}_q \otimes A_{311}$ where $\mathbf{1}_q \in \mathbb{R}^q$ is a vector of ones, and A_{311} is a row vector with $n-r$ elements. Then applying the coordinate transformation $x_p \mapsto x$ where $x = T_a x_p$ to (6), yields

$$\begin{aligned}\underbrace{\begin{bmatrix}\dot{x}_1(t)\\ \dot{x}_2(t)\\ \dot{z}_f(t)\end{bmatrix}}_{\dot{x}_a(t)} &= \underbrace{\begin{bmatrix}A_{11}(\rho) & A_{12}(\rho) & 0\\ A_{21}(\rho) & A_{22}(\rho) & 0\\ A_{31} & A_{32} & -A_f\end{bmatrix}}_{A(\rho)}\underbrace{\begin{bmatrix}x_1(t)\\ x_2(t)\\ z_f(t)\end{bmatrix}}_{x_a(t)} + \underbrace{\begin{bmatrix}T_s B_p(\rho)\\ 0\end{bmatrix}}_{B(\rho)}u(t) + \underbrace{\begin{bmatrix}0\\ A_f\end{bmatrix}}_{D}f(t) + \underbrace{\begin{bmatrix}T_s M_p(\rho)\\ 0\end{bmatrix}}_{M(\rho)}\zeta(t)\\ y_a(t) &= Cx_a(t)\end{aligned} \tag{8}$$

where $x_1 \in \mathbb{R}^{n-r}$, $x_2 \in \mathbb{R}^r$ and

$$C = \begin{bmatrix}0 & I_r & 0\\ 0 & 0 & I_q\end{bmatrix} \tag{9}$$

Remark 3

Note the form in (8) is bespoke to this paper and arises from the very specific problem formulation considered here. In particular a very specific manipulation of the ordering of the ordering of the measurements has been made to create y_a from y_p.

Remark 4

The system in (8)–(9) is now in the form

$$\begin{aligned}\dot{x}_a(t) &= A(\rho)x_a(t) + B(\rho)u(t) + Df(t) + M(\rho)\zeta(t)\\ y_a(t) &= Cx_a(t)\end{aligned} \tag{10}$$

which has a more conventional unknown input observer (UIO) formulation (i.e. C is full row rank and CD has full column rank). This has been achieved by the specific creation of $y_a \in \mathbb{R}^{r+q}$ from

the measured output $y \in \mathbb{R}^p$. The sliding mode observer for (10) is therefore essentially similar to the one from [1, 2]. Some details are repeated here because specific assumptions need to be exploited and some subtle differences are present.

Assumption 3
In this paper, it is assumed that $(A_{11}(\rho), A_{21}(\rho))$ defined in (8) is detectable.

Remark 5
A sufficient condition to guarantee the observability/detectability for $(A_{11}(\rho), A_{21}(\rho))$ can be found in [23].

The proposed sliding mode observer has the structure

$$\underbrace{\begin{bmatrix}\dot{\hat{x}}_1(t)\\ \dot{\hat{x}}_2(t)\\ \dot{\hat{z}}_f(t)\end{bmatrix}}_{\dot{z}(t)} = \underbrace{\begin{bmatrix}A_{11}(\rho) & A_{12}(\rho) & 0\\ A_{21}(\rho) & A_{22}(\rho) & 0\\ A_{31} & A_{32} & -A_f\end{bmatrix}}_{A(\rho)} \underbrace{\begin{bmatrix}\hat{x}_1(t)\\ \hat{x}_2(t)\\ \hat{z}_f(t)\end{bmatrix}}_{z(t)} + \underbrace{\begin{bmatrix}T_s B_p(\rho)\\ 0\end{bmatrix}}_{B(\rho)} u(t) + G_l(\rho) e_y(t) + G_n \nu(t) \tag{11}$$
$$\hat{y} = Cz$$

where the output estimation error $e_y(t) = C(x_a(t) - z(t))$ and the output error injection is given by

$$\nu = \begin{cases} k(t)\dfrac{e_y}{\|e_y\|} & \text{if } e_y \neq 0 \\ 0 & \text{otherwise} \end{cases} \tag{12}$$

where $k(t)$ is a positive scalar. In (11), $\rho(t) \in \hat{\Theta} \subset \mathbb{R}^h$ and denotes the scheduling parameters of the SMO, where $\hat{\Theta}$ is a compact set. As in [2], the matrix $G_n \in \mathbb{R}^{(n+q)\times(q+r)}$ in (11) is given by

$$G_n = \begin{bmatrix} -L \\ I_{r+q} \end{bmatrix} \tag{13}$$

where the design matrix $L \in \mathbb{R}^{(n-r)\times(p+r)}$ has the structure

$$L = \begin{bmatrix} L_1 & 0 \end{bmatrix} \tag{14}$$

and the matrix $L_1 \in \mathbb{R}^{(n-r)\times r}$. *Note the dimensions of $G_l(\rho)$ and G_n are bespoke to this paper and are quite different to the generic case in [2], [15].* Here because of the redundancy and hence the rank deficiency in C_p, the sliding motion is no longer order n.

In the sequel partition $M(\rho)$ as

$$M(\rho) = \begin{bmatrix} M_1(\rho) \\ M_2(\rho) \end{bmatrix} \tag{15}$$

where $M_1(\rho) \in \mathbb{R}^{(n-r)\times d}$ and

$$M_2(\rho) = \begin{bmatrix} M_{21}(\rho) \\ 0 \end{bmatrix} \in \mathbb{R}^{(r+q)\times d} \tag{16}$$

where $M_{21}(\rho) \in \mathbb{R}^{r\times d}$. This specific structure of uncertainty will be exploited later in the paper. Define $e = x_a - z$ and let $e = \text{col}(e_1, e_2, e_{zf})$ where $e_1 \in \mathbb{R}^{n-r}$, $e_2 \in \mathbb{R}^r$ and $e_{zf} \in \mathbb{R}^q$. Then subtracting (8) from (11) yields

$$\begin{bmatrix} \dot{e}_1 \\ \dot{e}_2 \\ \dot{e}_{zf} \end{bmatrix} = \left[\begin{array}{c|c|c} A_{11}(\rho) & A_{12}(\rho) & 0 \\ \hline A_{21}(\rho) & A_{22}(\rho) & 0 \\ \hline A_{31} & A_{32} & -A_f \end{array}\right] \begin{bmatrix} e_1 \\ e_2 \\ e_{zf} \end{bmatrix} + \begin{bmatrix} 0 \\ D_2 \end{bmatrix} f - \begin{bmatrix} G_{l1}(\rho) \\ G_{l2}(\rho) \end{bmatrix} e_y - \begin{bmatrix} -L \\ I_{r+q} \end{bmatrix} \nu + \begin{bmatrix} M_1(\rho) \\ M_2(\rho) \end{bmatrix} \zeta \tag{17}$$

where the gain $G_l(\rho)$ has been appropriately partitioned, and the matrix $D_2 \in \mathbb{R}^{(r+q)\times q}$ is given by

$$D_2 = \begin{bmatrix} 0 \\ A_f \end{bmatrix} \tag{18}$$

Define a coordinate transformation $e \mapsto T_L e = \tilde{e}$, given by

$$T_L = \begin{bmatrix} I_{n-r} & L \\ 0 & I_{r+q} \end{bmatrix} \tag{19}$$

Applying the above transformation to (17) and using the fact that $LD_2 = 0$ (because of the structures of L from (14) and D_2 from (18)) generates a new error coordinate system

$$\underbrace{\begin{bmatrix} \dot{\tilde{e}}_1 \\ \dot{\tilde{e}}_2 \\ \dot{\tilde{e}}_{zf} \end{bmatrix}}_{\dot{\tilde{e}}} = \left[\begin{array}{c|c|c} \tilde{A}_{11}(\rho) & \tilde{A}_{12}(\rho) & 0 \\ \hline A_{21}(\rho) & \tilde{A}_{22}(\rho) & 0 \\ \hline A_{31} & \tilde{A}_{32} & -A_f \end{array}\right] \underbrace{\begin{bmatrix} \tilde{e}_1 \\ \tilde{e}_2 \\ \tilde{e}_{zf} \end{bmatrix}}_{\tilde{e}} + \begin{bmatrix} 0 \\ D_2 \end{bmatrix} f - \begin{bmatrix} \tilde{G}_{l1}(\rho) \\ G_{l2}(\rho) \end{bmatrix} e_y - \begin{bmatrix} 0 \\ I_{r+q} \end{bmatrix} \nu + \underbrace{\begin{bmatrix} \tilde{M}_1(\rho) \\ M_2(\rho) \end{bmatrix}}_{\tilde{M}(\rho)} \zeta \tag{20}$$

where $\tilde{e}_1 = e_1 + L_1 e_2$ and $\tilde{G}_{l1}(\rho) = G_{l1}(\rho) + LG_{l2}(\rho)$. As a result of the change of coordinates in (20)

$$\begin{aligned} \tilde{A}_{11}(\rho) &= A_{11}(\rho) + L_1 A_{21}(\rho) \\ \tilde{A}_{22}(\rho) &= A_{22}(\rho) - A_{21}(\rho) L_1 \\ \tilde{A}_{32} &= A_{32} - A_{31} L_1 \\ \tilde{M}_1(\rho) &= M_1(\rho) + L_1 M_{21}(\rho) \end{aligned} \tag{21}$$

Exploiting Assumption 3, the matrix design freedom L is selected to ensure $\tilde{A}_{11}(\rho)$ is quadratically stable, i.e. there exists a symmetric positive definite matrix P_1 such that

$$P_1 \tilde{A}_{11}(\rho) + \tilde{A}_{11}(\rho)^T P_1 < 0 \tag{22}$$

Note that despite this change of coordinates the matrix A_{31} remains unaffected (and comprises q identical rows whose elements are the row vector A_{311}).

Define

$$\tilde{A}_{21}(\rho) = \begin{bmatrix} A_{21}(\rho) \\ A_{31} \end{bmatrix} \tag{23}$$

where $A_{31} \in \mathbb{R}^{q\times(n-r)}$ and does not depend on the scheduling parameter. This follows because the lower left sub-block of $A(\rho)$ in (11) is independent of the scheduling parameter. This property is preserved despite the sequence of transformations used to establish (20). This structure is exploited in the sequel.

In the error system coordinates in (20) define

$$\left[\begin{array}{c} \tilde{G}_{l1}(\rho) \\ \hline G_{l2}(\rho) \end{array}\right] = \left[\begin{array}{cc} \tilde{A}_{12}(\rho) & 0 \\ \hline \tilde{A}_{22}(\rho) + k_2 I_r & 0 \\ \tilde{A}_{32} & -A_f + k_2 I_q \end{array}\right] \tag{24}$$

where k_2 is a positive design scalar. The following result pertains to the existence of a sliding motion and establishes conditions on the modulation gain $k(t)$ in (12).

Define a sliding surface in the state estimation error space as

$$\mathcal{S} = \{\tilde{e} \in \mathbb{R}^{n+q} : C\tilde{e} = 0\} \tag{25}$$

where C is defined in (9).

Theorem 1

Provided the modulation gain k is suitably larger than the fault, a sliding motion on $\mathcal{S}$ can be enforced in finite time.

Proof

Substituting (24) into (20) yields

$$\dot{\tilde{e}} = \tilde{A}_e(\rho)\tilde{e} + \begin{bmatrix} 0 \\ D_2 \end{bmatrix} f + \tilde{M}(\rho)\zeta - \begin{bmatrix} 0 \\ I_{r+q} \end{bmatrix} \nu \tag{26}$$

where

$$\tilde{A}_e(\rho) = \begin{bmatrix} \tilde{A}_{11}(\rho) & 0 \\ \tilde{A}_{21}(\rho) & -k_2 I_{r+q} \end{bmatrix} \text{ and } \tilde{M}(\rho) = \begin{bmatrix} \tilde{M}_1(\rho) \\ M_2(\rho) \end{bmatrix} \tag{27}$$

Let $P_1 \in \mathbb{R}^{(n-r)\times(n-r)}$ be a symmetric strictly positive definite matrix such that (22) holds. Then for a sufficiently large positive gain k_2, the symmetric positive definite matrix $P = \mathrm{diag}(P_1, I_{r+q})$ has the property that

$$P\tilde{A}_e(\rho) + \tilde{A}_e(\rho)^T P < 0 \tag{28}$$

For details see for example [24]. Note that (22) and (28) can be evaluated and tested at all vertices of the polytope. Exploiting the fact that the signals f and ζ are bounded, and by construction

$$\tilde{e}^T P \begin{bmatrix} 0 \\ I_{r+q} \end{bmatrix} \nu = k(t)\|e_y\| \tag{29}$$

it follows using the Lyapunov function $V(\tilde{e}) = \tilde{e}^T P \tilde{e}^T$ that if $k > \|f\|$, $\dot{V} \leq P\tilde{A}_e(\rho) + \tilde{A}_e(\rho)^T P + 2\tilde{e}^T \tilde{M}(\rho)\zeta$. Since $\|\zeta\|$ is bounded, it follows that $\tilde{e}(t)$ in (26) is ultimately bounded and so $\tilde{e}_1(t)$ is also ultimately bounded. Suppose for $t > t_0$, $\|\tilde{e}(t)\| < \chi$ and define

$$a_{21} = \max_{\rho \in \Theta} \|\tilde{A}_{21}(\rho)\|, \quad m_2 = \max_{\rho \in \Theta} \|M_2(\rho)\| \tag{30}$$

Then choosing

$$k = a_{21}\chi + k_2\|e_y\| + \|D_2\|\|f\| + m_2\beta + \eta \tag{31}$$

where β is the bound on the uncertainty $\zeta(t)$ and η is a positive scalar, it follows that

$$\begin{aligned} e_y^T \dot{e}_y &= e_y^T(\tilde{A}_{21}(\rho)\tilde{e}_1 - k_2 e_y + D_2 f + M_2(\rho)\zeta - \nu) \\ &\leq \|e_y\|(a_{21}\chi + k_2\|e_y\| + \|D_2\|\|f\| + m_2\beta - k) \\ &\leq -\eta\|e_y\| \end{aligned} \tag{32}$$

This ensures sliding takes place on $\mathcal{S}$ in finite time and can be maintained on $\mathcal{S}$ in the face of faults [25]. □

Remark 6

Note that Theorem 1 demonstrates that the detectability of $(A_{11}(\rho), A_{21}(\rho))$ implies detectability of $(A(\rho), C)$ as a consequence of (28).

2.2. Fault reconstruction

During sliding on $\mathcal{S}$, $\dot{\tilde{e}}_2(t) = \tilde{e}_2(t) = 0$ and $\dot{\tilde{e}}_{zf}(t) = \tilde{e}_{zf}(t) = 0$. Let

$$\nu_{eq} = \begin{bmatrix} \nu_{eq,1} \\ \nu_{eq,2} \end{bmatrix} \tag{33}$$

where ν_{eq} is the equivalent output error injection signal necessary to maintain sliding and $\nu_{eq,1} \in \mathbb{R}^r$ and $\nu_{eq,2} \in \mathbb{R}^q$.

During sliding, (20) can be rewritten as

$$\dot{\tilde{e}}_1 = \tilde{A}_{11}(\rho)\tilde{e}_1 + \tilde{M}_1(\rho)\zeta \tag{34}$$

$$0 = A_{21}(\rho)\tilde{e}_1 - \nu_{eq,1} + M_{21}(\rho)\zeta \tag{35}$$

$$0 = A_{31}\tilde{e}_1 + A_f f - \nu_{eq,2} \tag{36}$$

Equation (34) governs the dynamics of the sliding motion. The absence of uncertainty in (36) follows from the structure of $M_2(\rho)$ in (16). In order to reduce the effect of the unmatched uncertainty ζ on $\tilde{e}_1$, whilst ensuring stability of the reduced order sliding motion, L_1 is selected to minimise the $\mathcal{L}_2$ norm γ associated with the LPV system $H(\rho) : \zeta \mapsto \xi$ given by

$$H(\rho) : \begin{cases} \dot{\tilde{e}}_1 = \tilde{A}_{11}(\rho)\tilde{e}_1 + \tilde{M}_1(\rho)\zeta \\ \xi = A_{31}\tilde{e}_1 \end{cases} \tag{37}$$

Using the vertex property and the Bounded Real Lemma, L_1 can be calculated by solving a finite number of linear matrix inequalities (see for example [26, 27, 3]), specifically:

Theorem 2
An upper bound on the $\mathcal{L}_2$ gain γ for the LPV system $H(\rho)$ can be computed so that

$$\|\xi\|_{\mathcal{L}_2} \leq \gamma \|\zeta\|_{\mathcal{L}_2} \tag{38}$$

if there exists a s.p.d matrix P_0 and design freedom L_1 such that

$$\begin{bmatrix} P_0\tilde{A}_{11}(\rho) + \tilde{A}_{11}(\rho)^T P_0 & P_0\tilde{M}_1(\rho) & A_{31}^T \\ * & -\gamma I & 0 \\ * & * & -\gamma I \end{bmatrix} < 0 \tag{39}$$

Proof
From the Bounded Real Lemma, (38) is guaranteed if (39) holds. Using the vertex property discussed in [26], the representation in (39) can be converted into polytopic form and the synthesis of L and the analysis of (39) is undertaken only at the vertices of the polytope. Writing $Y = P_0 L$ it follows (39) is affine with respect to the decision variables P_0 and Y. □

Corrolary 1. In the absence of uncertainty i.e. when $\xi = 0$ then $\tilde{e}_1 \to 0$ as $t \to \infty$ and

$$\hat{f} = A_f^{-1} \nu_{eq,2} \tag{40}$$

is an asymptotic estimate of the fault.

Proof
In the absence of uncertainty, (34) reduces to $\dot{\tilde{e}}_1 = \tilde{A}_{11}(\rho)\tilde{e}_1$ and $\tilde{e}_1 \to 0$ as $t \to \infty$ as claimed. Since $\tilde{e}_1 \to 0$ as $t \to \infty$, it follows from (36) that $\nu_{eq,2} \to A_f f$ as $t \to \infty$. □

In the presence of uncertainty, if the fault reconstruction $\hat{f}$ is chosen as in (40), however it is clear from (36) that the fault reconstruction signals $\hat{f}$ will be affected by the unmatched uncertainty since $\tilde{e}_1$ is driven by the uncertainty ζ.

3. ISOLATION LOGIC

In this section, fault isolation logic is discussed in the presence of uncertainty according to two fault scenarios.

3.1. All redundant sensors are faulty

In this situation, the ith fault reconstruction signal $\hat{f}_i$ for $i = 1, \ldots, q$, calculated using (40), reflects information about both the faults and the unmatched uncertainty in the ith channel. The signal $\hat{f}_i$ can still be used directly for FDI purposes provided the unmatched uncertainty is small enough compared with the fault in the ith channel (This is effectively the problem considered in the earlier work [2]).

3.2. One redundant sensor is fault free

Without loss of generality, assume the qth redundant sensor is fault-free and the remaining $q-1$ redundant sensors are assumed to be faulty.
As defined in (5), the diagonal elements in A_f are denoted by a_f and let the equivalent output error injection associated with the ith channel be $\nu_{eq2,i}$. Then using (40), the ith fault reconstruction signal is given by

$$\hat{f}_i = a_f^{-1}\nu_{eq2,i} \;\; \forall i = 1, \ldots, q \tag{41}$$

The equivalent error injection signals associated with the faulty channels are given by

$$\nu_{eq2,i} = A_{311}\tilde{e}_1 + a_f f_i \;\; \forall i = 1, \ldots, q-1 \tag{42}$$

where A_{311} represents one of the repeated row vectors in A_{31} and f_i denotes the actual fault occurring in the ith channel. Substituting (42) into (41) yields

$$\hat{f}_i = a_f^{-1}A_{311}\tilde{e}_1 + f_i \;\; \forall i = 1, \ldots, q-1 \tag{43}$$

Obviously, the fault reconstruction performance is degraded due to the term $a_f^{-1}A_{311}\tilde{e}_1$. Now considering that the qth redundant sensor is fault free, i.e. $f_q = 0$, it follows from (36) that

$$v_{eq2,q} = A_{311}\tilde{e}_1 \tag{44}$$

Substituting (44) into (40) yields $\hat{f}_q = a_f^{-1}A_{311}\tilde{e}_1$ and reconstructs the uncertainty in (43). Using (43), a 'clean' fault reconstruction signal $\tilde{f}_i$ is given by

$$\tilde{f}_i = \hat{f}_i - \hat{f}_q = f_i \;\; \text{for all} \;\; i = 1, \ldots, q-1 \tag{45}$$

Remark 7
It is clear from (45) that the unmatched uncertainty term $a_f^{-1}A_{311}\tilde{e}_1$ can be cancelled in all faulty channels if fault free sensor redundancy is available. Then the 'clean' fault reconstruction signals $\tilde{f}_i$ will be used for FDI purposes. It is therefore crucial to be able to identify fault free injection signals. This will be discussed in the next section.

4. FAULT RECONSTRUCTION DECISION MAKING LOGIC

This section discusses the decision making logic used to create the claimed improved fault reconstruction performance in the presence of a fault free redundant sensor.
Without loss of generality, assume the qth redundant sensor is fault free, in which case it can be assumed that the magnitude of $\hat{f}_q$ is smaller than $\hat{f}_i, i = 1, \ldots, q-1$. Then 'clean' fault reconstruction signals $\tilde{f}_i, i = 1, \ldots, q-1$ are calculated using (45).
Further, partition $y_{p,2}$ as

$$y_{p,2} = \left[y_{p2,1}, \ldots, y_{p2,q}\right]^T \tag{46}$$

and let

$$\tilde{y}_{p,2} = \begin{bmatrix} \tilde{y}_{p2,1} \\ \vdots \\ \tilde{y}_{p2,q-1} \\ \tilde{y}_{p2,q} \end{bmatrix} = \begin{bmatrix} y_{p2,1} - \tilde{f}_i \\ \vdots \\ y_{p2,q-1} - \tilde{f}_{q-1} \\ y_{p2,q} \end{bmatrix} \tag{47}$$

where $y_{p2,q}$ represents the qth redundant sensor output which is fault free. If

$$\tilde{y}_{p2,1} \approx \tilde{y}_{p2,2} \approx \ldots \approx \tilde{y}_{p2,q} \tag{48}$$

then it is confirmed that a) the fault free measurement has been correctly identified b) that the reconstruction signals $\tilde{f}_i$ for $i = 1, \ldots, q-1$ denotes an improved fault estimation compared with $\hat{f}_i$ for $i = 1, \ldots, q-1$.

5. RECONFIGURE BENCHMARK CASE STUDY

The RECONFIGURE benchmark is a *nonlinear highly representative model* of a generic Airbus civil commercial aircraft [16, 28]. The benchmark contains a baseline gain-scheduled controller, detailed actuator and sensor models, as well as angle of attack and speed protection components and measurement filters. This aircraft model, which has been developed within the EU funded RECONFIGURE project, is used as the basis for all the scenarios and for testing different fault detection and fault tolerant control strategies. Simplified LPV models are also available for the *design* of FDI and fault tolerant control schemes [16, 28].

An LPV model of the benchmark has been established using polynomial interpolation of multiple longitudinal linear time invariant models linearized under cruise conditions. The chosen scheduling parameters are

$$\rho = \begin{bmatrix} w(\text{tons}) & cg(\%) & V_c(\text{kt}) & M_a \end{bmatrix} \tag{49}$$

which represent the aircraft weight, the centre of gravity position, calibrated airspeed and Mach number. The scheduling parameters have been normalized in the interval $\begin{bmatrix} 0 & 1 \end{bmatrix}$. All parameter-varying matrices are assumed to depend affinely on ρ, in particular $A(\rho) = A_0 + \sum_{i=1}^{4} \rho_i A_i$. In this paper, due to the existence of aggressive pitch stick excitations, significant plant-model mismatch exists. The plant-model mismatch will be dealt with by ensuring the occurrence of a sliding mode [29] and fully utilising the sensor redundancy. This is another advantage of the proposed scheme. The state variables are

$$x_p = \begin{bmatrix} q & p & V_g & \alpha & \theta & Z_g \end{bmatrix}^T \tag{50}$$

representing pitch rate, roll rate, ground speed, angle of attack, pitch and altitude respectively.

Table I. Flight points on the edge of the flight envelope

Flight Points	Gross weight (t)	CG(%)	VCAS (kt)	Zg(ft)	S/F conf	Landing gear	Phase
A	MFW	Max forward CG	VLS-5	Ceiling	0	Up	2
B	MFW	Medium CG	VFE	1000	4	Down	2
C	(MTOW+MLW)/2	Max aft CG	VLS-5	Ceiling	0	Up	2
D	MTOW	Max aft CG	VFE	1000	4	Down	2

Suppose the system outputs are only partially measurable. Crucially, the variable V_g is also treated as 'unreliable' due to the potential loss of calibrated airspeed V_c. For the purpose of achieving the 'output canonical form', the output variables are reordered as

$$y_p = \left[\begin{array}{ccc|ccc} q & \theta & Z_g & \alpha_1 & \alpha_2 & \alpha_3 \end{array} \right]^T \tag{51}$$

where α_1, α_2 and α_3 represent angle of attack measured by three individual air data sensors (before the consolidation logic in the air data inertial reference system ADIRS) each of which are assumed to be potentially corrupted by sensor faults. The system input vector is $u_p = \left[\begin{array}{cc} \delta_e & \delta_{stab} \end{array} \right]^T$ where δ_e denotes an aggregation of the control deflections of the elevators (which are assumed to move in tandem) and δ_{stab} represents the stabilizer deflection.

The proposed scheme will be evaluated at four edges of the flight envelope, which are listed in Table II (see bottom of the page) wherein 'MFW', 'MLW' and 'MTOW' denote the maximum flight weight, the maximum landing weight and the maximum take-off weight, respectively, and 'VLS' and 'VFE' represent the minimum selectable speed and the maximum speed slat/flap extended, respectively. The numerical values with respect to the various weights and speeds are not given in this paper due to industrial restrictions.

The pitch stick excitation associated with the four flight conditions are shown in Fig. 2. In the example, 3deg and 5deg sensor biases (faults) are assumed to occur on α_1 and α_2, respectively (i.e. the first two measurements of angle of attack). The third redundant sensor associated with α_3 is assumed to be fault free. Furthermore, the fault signals f_1 and f_2 are assumed to occur simultaneously at 5sec. To facilitate the industrial evaluation of the computational load of the

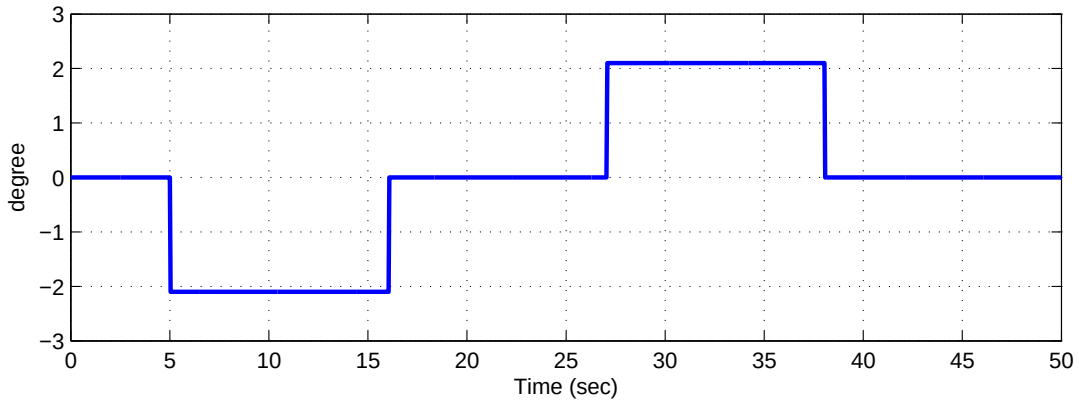

Figure 2. Pitching stick excitation

design, the FDD scheme proposed in this paper has been re-coded purely based on the Airbus state of practice for Flight Control Computer (FCC) software coding – the SAO (Airbus software, Computer-Assisted Specification) library [18]. This contains a set of graphical functional blocks (in the manner of SIMULINK blocks), allowing only a limited set of mathematical operations. For each SAO block, a specific computational load is defined. Through classifying and counting the SAO blocks used the FDD scheme, the associated computational load is calculated.

Due to industrial limitations, the numerical 'SAO' coding results are not provided straightforwardly. As in (52), the 'scaled' computational load is treated as a criteria to measure Airbus's 'industrial complexity'. Specifically

$$ET_s = \frac{ET}{ET_{max}} \tag{52}$$

where ET_s represents the 'scaled' computational load which is defined as a ratio between the actual computational load ET and the maximum allowable computational load ET_{max} predefined by Airbus.

Table II shows the scaled 'SAO' coding results associated with the FDI scheme in this paper and the one used in [15]. Clearly, the proposed FDI scheme has much lower SAO computational burden.

Table II. Comparison of the scaled industrial computational load

	Proposed FDI scheme	FDI scheme in [15]
ET_s	0.376208	2.317008

5.1. *Design results*

In this example, $n = 6; p = 6, q = 3$ and

$$C_p = \begin{bmatrix} C_{p,1} \\ \hline C_{p,2} \end{bmatrix} = \left[\begin{array}{cccccc} 1 & 0 & 0 & 0 & 0 & 0 \\ 0 & 0 & 0 & 0 & 1 & 0 \\ 0 & 0 & 0 & 0 & 0 & 1 \\ \hline 0 & 0 & 0 & 1 & 0 & 0 \\ 0 & 0 & 0 & 1 & 0 & 0 \\ 0 & 0 & 0 & 1 & 0 & 0 \end{array}\right] \quad N_p = \begin{bmatrix} 0 & 0 & 0 \\ 0 & 0 & 0 \\ 0 & 0 & 0 \\ 1 & 0 & 0 \\ 0 & 1 & 0 \\ 0 & 0 & 1 \end{bmatrix}$$

By choosing a suitable gain matrix for L_1 in (13) and (14), the matrix $\tilde{A}_{11}(\rho)$ is established. In this design, $k = 3$, $A^s_{22} = I_3$ and the value of L has been obtained using the Matlab LMI toolbox as

$$L = \begin{bmatrix} 0.0034 & 0 & 0.5334 & 0 & 0 & 0 \\ 0.0000 & 0 & 0.0028 & 0 & 0 & 0 \\ 0.0070 & 0 & 1.5471 & 0 & 0 & 0 \end{bmatrix} \tag{53}$$

The filter parameter $A_f = I_3$, the scalar ϱ is 13, and the small positive scalar selected for the sigmoidal approximation [25] to the discontinuous injection term is 0.01.

5.2. *Simulation results*

During the simulation, the auto-trust is engaged during the whole simulation. Since unexpected closed-loop behaviour will occur under some flight conditions due to the existence of uncompensated sensor bias, the fault reconstruction performance will be degraded and 'perfect' fault reconstruction is difficult to achieve. The behaviours of the aircraft states are not shown here due to industrial restrictions.

The sliding surfaces $\|e_y\|$ associated with the four flight conditions are shown in Fig. 3. Despite some flight conditions being on the edge of the flight envelope, $\|e_y\|$ is close to zero and sliding is maintained.

The comparisons between the actual sensor bias acting on α_1 and α_2, the fault reconstruction signals and the clean fault reconstruction signals, associated with four flight conditions, are shown in Figs. 4-7. In Figs. 4-7, the red lines represents the actual sensor bias. The blue and green lines depict the fault reconstruction signals (i.e. $\hat{f}_1$ and $\hat{f}_2$) and the 'clean' fault reconstruction signals $\tilde{f}_1$ and $\tilde{f}_2$ (as defined in Section 3), respectively. It is clear from Figs. 4-7 that all the fault reconstruction signals approximate the correct magnitudes of the two sensor biases (despite being tested over a wide set of flight conditions and in the presence of unexpected closed-loop behaviour caused by the uncompensated sensor biases being fed to the controller), and therefore fault isolation can be achieved. Furthermore, the fault reconstruction performance is improved by using the redundant fault free sensor to create 'clean' fault estimates $\tilde{f}_i$. *These 'clean' estimates $\tilde{f}_i$ are always better than their original counterparts $\hat{f}_i$.*

The fault reconstruction performance is judged using the decision making logic provided in Section 4. Absolute values of errors between $\tilde{y}_{p2,1}$, $\tilde{y}_{p2,2}$ and $\tilde{y}_{p2,3}$ are shown in Fig. 8. It is clear from Fig. 8 that the fault reconstruction performance is good despite the wide range of flight conditions. Spikes at 5sec are caused by the occurrence of the sensor bias.

6. CONCLUSION

This study has proposed a sliding mode sensor FDI scheme wherein the triplex sensor redundancy is utilised to achieve FDI directly, so that minimal additional logic and post-processing is required to isolate the location of the faults. To achieve this, a slightly nonstandard sliding mode observer formulation has been introduced account for the fact that not all of the measurements, in a system theory sense, are independent. Because of this special formulation, and the absence of any extensive post-processing, the computational burden of the proposed observer scheme is greatly reduced compared to earlier work. To achieve this, the equivalent output error injection signal associated with the fault free redundant sensor can be used to improve the fault reconstruction performance. The fault isolation logic and decision making logic used to create the fault reconstructions are also discussed. The proposed scheme is has been applied to the RECONFIGURE benchmark model to simultaneously detect and isolate two types of sensor bias which act simultaneously on two angle of attack sensor measurements. Good fault reconstruction results demonstrate the efficacy of the proposed scheme.

ACKNOWLEDGEMENT

This work is supported by the EU Grant (FP7-AAT-2012-314544): RECONFIGURE.

REFERENCES

1. Alwi H, Edwards C, Marcos A. Fault reconstruction using a LPV sliding mode observer for a class of LPV systems. *J. Franklin Inst.* 2012; **349**:510–530.
2. Alwi H, Edwards C. Robust fault reconstruction for linear parameter varying systems using sliding mode observers. *Int J Robust Nonlinear Control* 2014; **24**:1947–1968, doi:DOI:10.1002/rnc.3009.
3. Wei X, Verhaegen M. LMI solutions to the mixed H_-/H_∞ fault detection observer design for linear parameter-varying systems. *Int. J. Adapt. Control Signal Process.* 2011; **25(2)**:114–136.
4. Patton R, Chen L. An LPV pole-placement approach to friction compensation as an FTC problem. *International Journal of Applied Mathematics and Computer Sciences* 2012; **22**:149–160.
5. Rodrigues M, Hamdi H, Braiek N, Theilliol D. Observer-based fault tolerant control design for a class of LPV descriptor systems. *J. Franklin Inst.* 2014; .
6. Vanek B, Edelmayer A, Szabo Z, Bokor J. Bridging the gap between theory and practice in LPV fault detection for flight control actuators. *Control Eng. Pract.* 2014; **31**:171–182.
7. Blesa J, Puig V, Bolea Y. Fault detection using interval LPV models in an open-flow canal. *Control Eng. Pract.* 2010; **18**:460–470.
8. Varga A, Hecker S, Ossmann D. Diagnosis of actuator faults using LPV-gain scheduling techniques. *AIAA Guidance, Navigation and Control Conference and Exhibit*, 2011.
9. Henry D. Structured fault detection filters for LPV systems modeled in an LFT manner. *Int. J. Adapt. Control Signal Process.* 2012; **26**:190–207.
10. Sato M. Filter design for LPV systems using quadratically parameter-dependent Lyapunov functions. *Automatica* 2006; **42**:2017–2023.
11. Chen L, Patton R, Goupil P. Robust fault estimation using an LPV reference model: ADDSAFE benchmark case study. *Control Eng. Pract.* 2016; **49**:194–203.
12. Bara GI, Daafouz J, Kratz F, Ragot J. Parameter-dependent state observer design for affine LPV systems. *Int. J. Control* 2001; **74**:1601–1611.
13. Briat C, Sename O, Lafay JF. Design of LPV observers for LPV time-delay systems: an algebraic approach. *Int. J. Control* 2011; **84**:1533–1542.
14. Alwi H, Edwards C. An adaptive sliding mode differentiator for actuator oscillatory failure case reconstruction. *Automatica* 2013; **49**:642–651.
15. Alwi H, Edwards C. Development and application of sliding mode LPV fault reconstruction schemes for the ADDSAFE Benchmark. *Control Eng. Pract.* 2014; **31**:148–170.
16. Goupil P, Boada-Bauxell J, Marcos A, Cortet E, Kerr M, Costa H. AIRBUS efforts toward advanced real-time fault diagnosis and fault tolerant control. *19th IFAC World Congress*, 2014.
17. Chen L, Edwards C, Alwi H. LPV sliding mode observers for sensor fault reconstruction with erroneous scheduling parameter measurements. *Proceedings of the IEEE CDC*, Osaka, Japan, 2015.
18. Goupil P. AIRBUS state of the art and practices on FDI and FTC in flight control system. *Control Eng. Pract.* 2011; **19**:524 – 539.
19. Goupil P. Oscillatory failure case detection in the A380 electrical flight control system by analytical redundancy. *Control Eng. Pract.* 2010; **18(9)**:1110–1119.
20. Goupil P, Marcos A. Advanced diagnosis for sustainable flight guidance and control: The European ADDSAFE project. *SAE technical paper*, 2011.
21. Goupil P, Puyou G. A high fidelity AIRBUS benchmark for system fault detection and isolation and flight control law clearance. *4th European Conference for Aerospace Sciences*, Saint Petersburg, Russia, 2011.
22. Goupil P, Marcos A. The European ADDSAFE project: Industrial and academic efforts towards advanced fault diagnosis. *Control Eng. Pract.* 2014; **31**:109–125.
23. Bokor J, Balas G. Linear parameter varying systems: A geometric theory and applications. *16th IFAC World Congress*, 2005; 12–22.
24. Edwards C, Yan X, Spurgeon SK. On the solvability of the constrained Lyapunov problem. *IEEE Trans. Automat. Contr.* 2007; **52**:1982–1987.
25. Utkin V. *Sliding modes in control and optimization*. Springer, 1992.
26. Apkarian P, Gahinet P, Becker G. Self-scheduled H_∞ control of linear parameter-varying systems: a design example. *Automatica* 1995; **31**(9).
27. Sato M, Peaucelle D. Gain-scheduled output-feedback controllers using inexact scheduling parameters for continuous-time LPV systems. *Automatica* 2013; **49**:1019–1025.
28. Goupil P, Boada-Bauxell J, Marcos A, Rosa P, Kerr M, Dalbies L. An overview of the FP7 RECONFIGURE project: Industrial, scientific and technological objectives. *SAFEPROCESS'15*, Paris, France, 2015.
29. Shtessel Y, Edwards C, Fridman L, Levant A. *Sliding mode control and observation*. Springer, 2013.

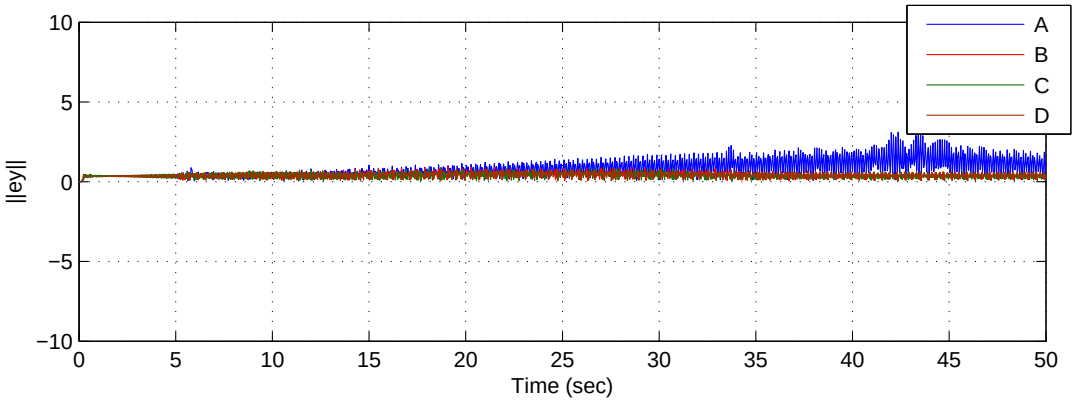

Figure 3. Sliding surfaces $\|e_y\|$

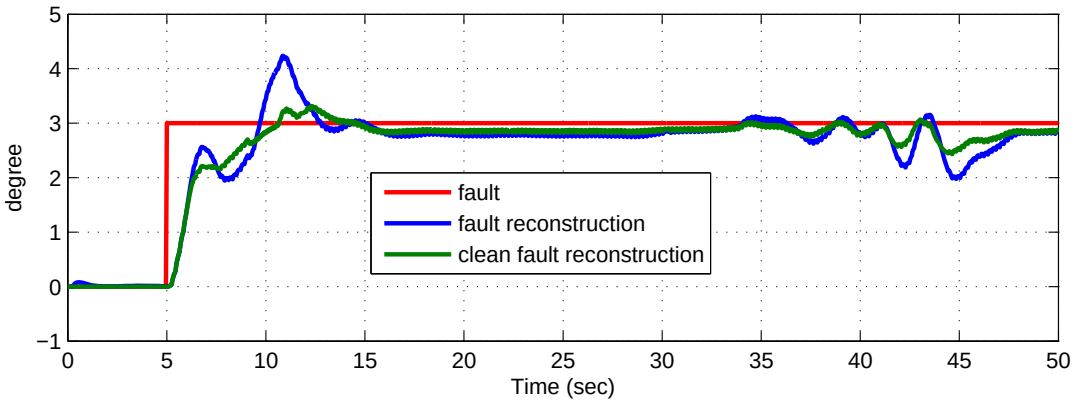

(a) Fault reconstruction performance associated with α_1

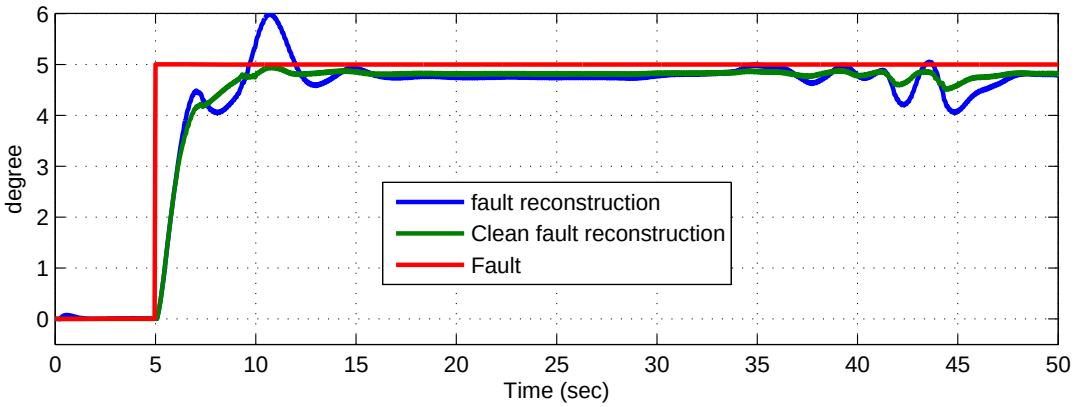

(b) Fault reconstruction performance associated with α_2

Figure 4. Flight point A

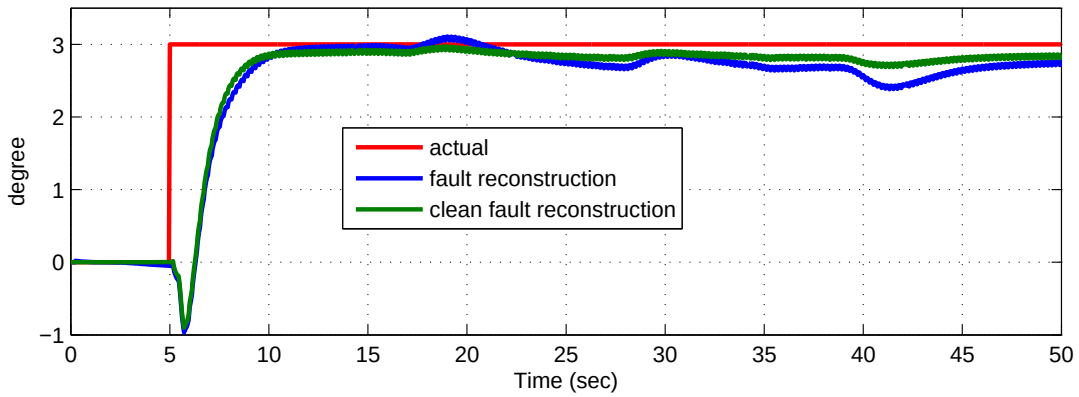

(a) Fault reconstruction performance associated with α_1

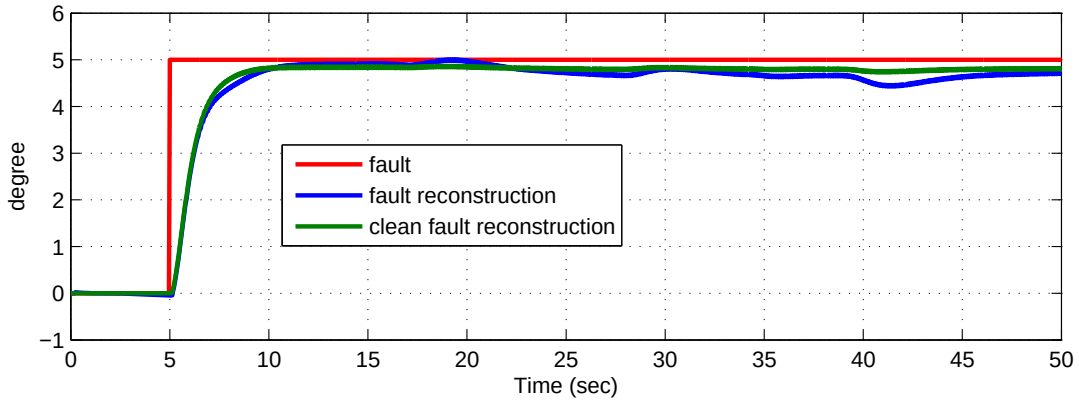

(b) Fault reconstruction performance associated with α_2

Figure 5. Flight point B

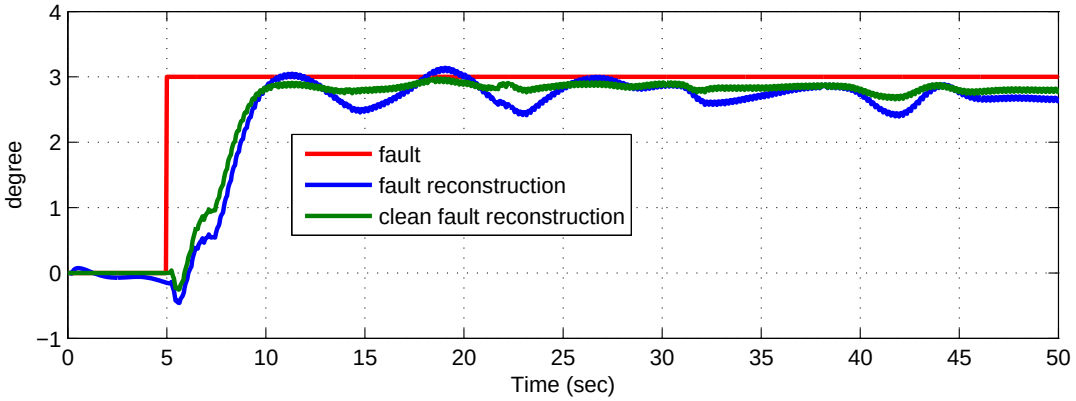

(a) Fault reconstruction performance associated with α_1

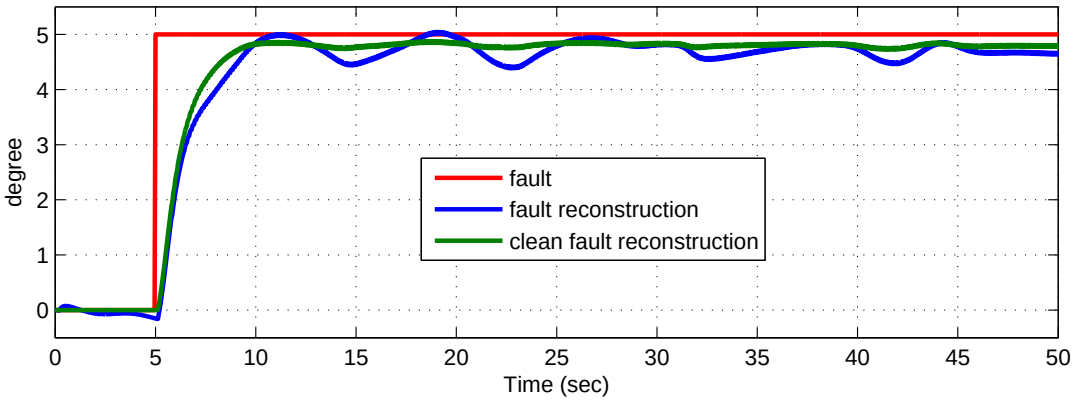

(b) Fault reconstruction performance associated with α_2

Figure 6. Flight point C

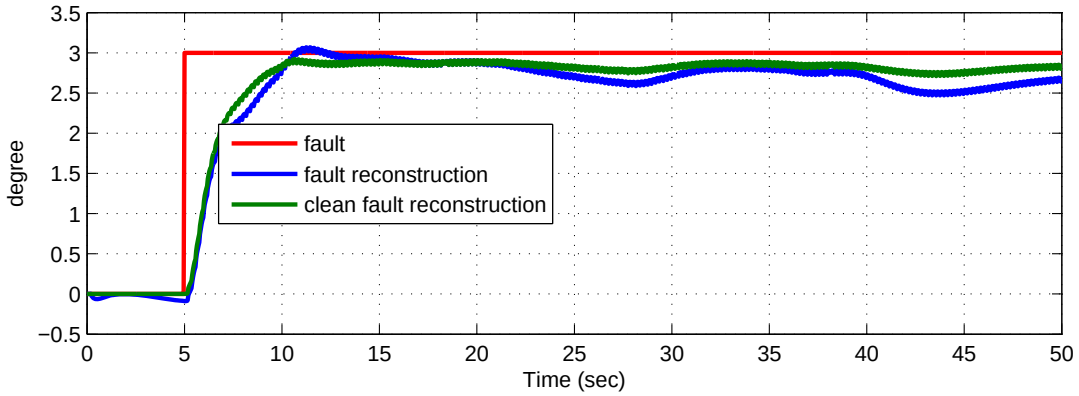

(a) Fault reconstruction performance associated with α_1

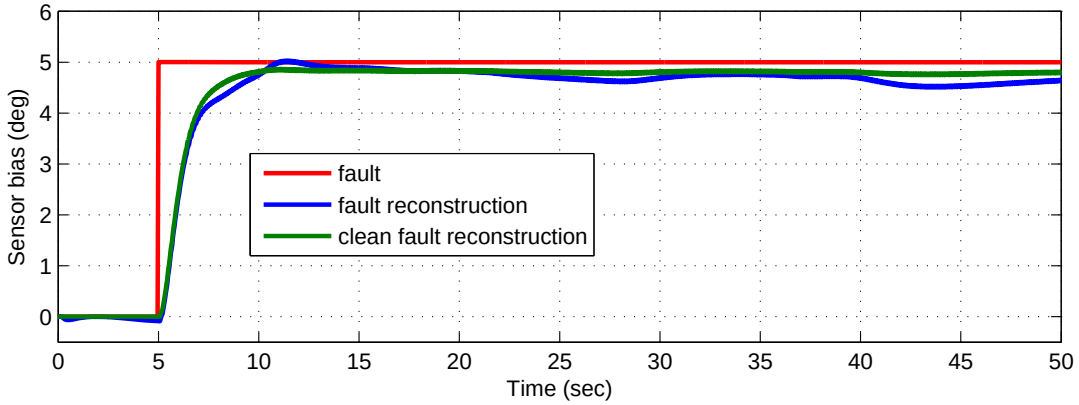

(b) Fault reconstruction performance associated with α_2

Figure 7. Flight point D

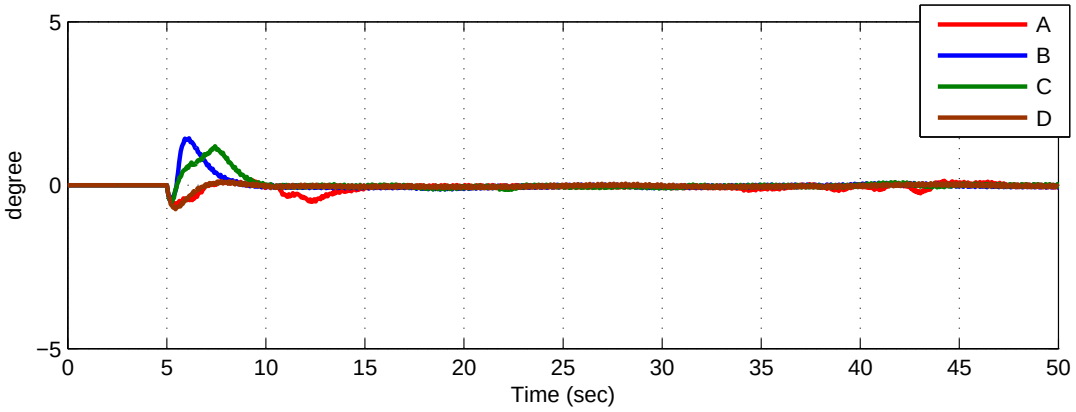

(a) errors between $\tilde{y}_{p2,1}$ and $\tilde{y}_{p2,2}$

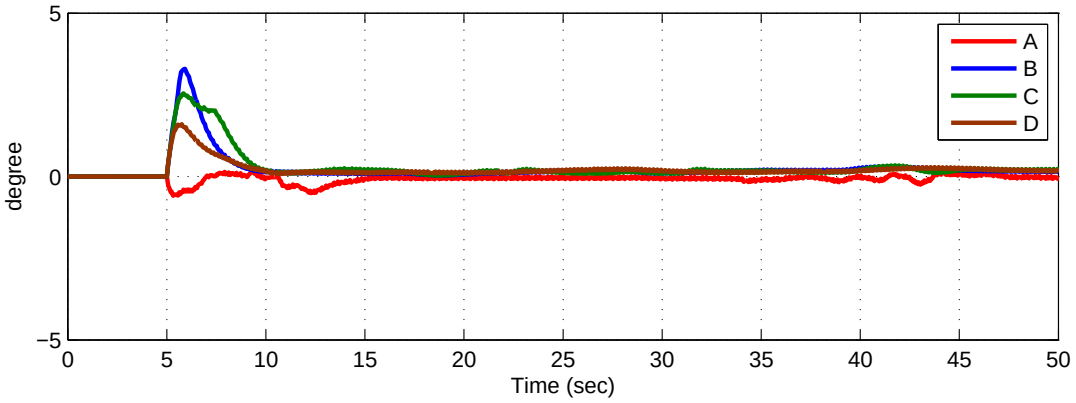

(b) errors between $\tilde{y}_{p2,1}$ and $\tilde{y}_{p2,3}$

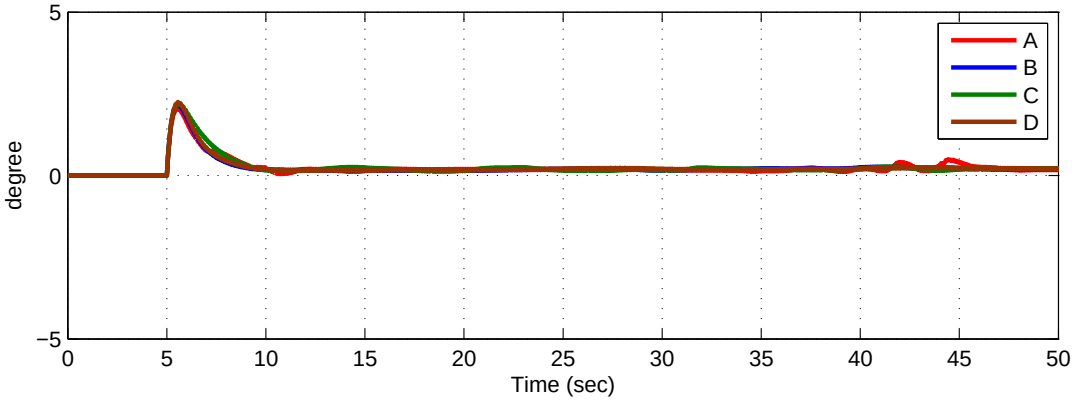

(c) errors between $\tilde{y}_{p2,2}$ and $\tilde{y}_{p2,3}$

Figure 8. Decision marking